



HAL
open science

Numerical analysis of the wall stress in abdominal aortic aneurysm influence of the material model incompressibility

Mamadou Toungara, Grégory Chagnon, Christian Geindreau

► To cite this version:

Mamadou Toungara, Grégory Chagnon, Christian Geindreau. Numerical analysis of the wall stress in abdominal aortic aneurysm influence of the material model incompressibility. *Journal of Mechanics in Medicine and Biology*, 2012, 12 (1), 10.1142/S0219519412004442 . hal-01974141

HAL Id: hal-01974141

<https://hal.science/hal-01974141>

Submitted on 10 Jan 2019

HAL is a multi-disciplinary open access archive for the deposit and dissemination of scientific research documents, whether they are published or not. The documents may come from teaching and research institutions in France or abroad, or from public or private research centers.

L'archive ouverte pluridisciplinaire **HAL**, est destinée au dépôt et à la diffusion de documents scientifiques de niveau recherche, publiés ou non, émanant des établissements d'enseignement et de recherche français ou étrangers, des laboratoires publics ou privés.

NUMERICAL ANALYSIS OF THE WALL STRESS IN ABDOMINAL AORTIC ANEURYSM: INFLUENCE OF THE MATERIAL MODEL NEAR-INCOMPRESSIBILITY

MAMADOU TOUNGARA, GREGORY CHAGON
and CHRISTIAN GEINDREAU*

*Laboratoire Sols — Solides — Structures — Risques
Université de Grenoble,
BP 53 — 38041 Grenoble Cedex 9, France
Christian.Geindreau@hmg.inpg.fr

Recently, hyperelastic mechanical models were proposed to well capture the aneurismal arterial wall anisotropic and nonlinear features experimentally observed. These models were formulated assuming the material incompressibility. However in numerical analysis, a nearly incompressible approach, i.e., a mixed formulation *pressure-displacement*, is usually adopted to perform finite element stress analysis of abdominal aortic aneurysm (AAA). Therefore, volume variations of the material are controlled through the volumetric energy which depends on the initial bulk modulus κ . In this paper, an analytical analysis of the influence of κ on the mechanical response of two invariant-based anisotropic models is first performed in the case of an equibiaxial tensile test. This analysis shows that for the strongly nonlinear anisotropic model, even in a restricted range of deformations, large values of κ are necessary to ensure the incompressibility condition, in order to estimate the wall stress with a reasonable precision. Finite element simulations on idealized AAA geometries are then performed. Results from these simulations show that the maximum stress in the AAA wall is underestimated in previous works, committed errors vary from 26% to 58% depending on the geometrical model complexity. In addition to affect the magnitude of the maximum stress in the aneurysm, we found that too small value of κ may also affect the location of this stress.

Keywords: Abdominal aortic aneurysm; anisotropic models; numerical analysis; near-incompressibility.

1. Introduction

In the last two decades, numerous numerical studies¹ have been performed in order to predict the wall stress distribution in abdominal aortic aneurysms (AAA), i.e., to predict the rupture of AAA. Accurate and reliable numerical stress analysis requires to take into account the geometrical features (tortuosity, asymmetry...) of AAA, the wall thickness, the presence of the intraluminal thrombus, the heterogeneity of

the wall, and the use of appropriate constitutive laws for the AAA material. The present work mainly concerns this last point. Like many soft tissues, the arterial wall is assumed to be an incompressible material namely in experimental studies. Under physiological conditions, this assumption could be justified.² The majority of published numerical studies in AAAs¹ have been performed using incompressible hyperelastic isotropic models fitted thanks to classical uniaxial tensile tests.³⁻⁶ However, biaxial tensile tests are more appropriate to characterize the anisotropic behavior of aneurismal arterial wall and for the development of suitable material models. In this way, planar biaxial tensile tests on normal and pathologic human abdominal aortic tissues were carried out in Ref. 7. The obtained results clearly show that the degeneration of the aorta leads to an increase in mechanical anisotropy and also an increase in the circumferential stiffness for AAA tissue as compared to normal aortic tissue. In order to take into account such features, hyperelastic anisotropic constitutive models were recently proposed using a Green-strain approach⁷ or an invariant approach.^{8,9} In both cases, the strain energy density W is formulated assuming that the arterial material is incompressible. These models were then implemented in a finite element code in order to compute both the distribution and the magnitude of stresses in patient-specific geometries using shell elements⁷ or in idealized AAA geometries⁸ using 3D elements. To perform such simulations, a nearly-incompressible approach, i.e., a mixed formulation *pressure-displacement* implemented in many finite element softwares, is usually adopted. For that purpose, the strain energy density W is split into an isochoric part \bar{W} and a volumetric part U : $W = \bar{W} + U$. The volumetric function U which depends on the jacobian J and on the initial bulk modulus κ of the material is used to control the volume variation.¹⁰ In practice, the incompressibility of the material is nearly reached for large values of κ which is used as a user-specified penalty parameter.

The main objective of the present work is to emphasize the influence of the initial bulk modulus κ values on both the magnitude and the distribution of the stress in an anisotropic AAA wall. To our knowledge, these values of κ as well as the form of the volumetric function $U(J)$ are rarely specified or discussed in previous numerical works. For that purpose, the paper is divided into two sections. In Sec. 2, an analytical analysis of compressibility effects on equibiaxial tensile tests is carried out. Two strain energies based on polynomial or exponential functions^{8,9} are considered and a classical quadratic volumetric function is used. Through a parametric study, the influence of the initial bulk modulus on the near-incompressibility of the mechanical response of the considered constitutive models is highlighted. Then, this influence is emphasized on idealized AAA geometrical models, in the last section. For that purpose the model proposed in Ref. 8 was implemented in a finite element code and numerical simulations on the AAA models were performed. The obtained results are finally compared to those in the literature.

2. Analytical Analysis of Compressibility Effects on Equibiaxial Tensile Tests

2.1. Material models

2.1.1. General framework

Hyperelastic models are often expressed thanks to strain elongations or strain invariants. The isotropic strain invariants I_1 , I_2 and I_3 (or J) are defined by:

$$I_1 = \text{tr}(\mathbf{C}), \quad I_2 = \frac{1}{2} [\text{tr}(\mathbf{C})^2 - \text{tr}(\mathbf{C}^2)], \quad I_3 = J^2 = \det(\mathbf{C}), \quad (1)$$

where $\mathbf{C} = \mathbf{F}^T \mathbf{F}$ is the right Cauchy–Green strain tensor and \mathbf{F} is the deformation gradient whose principal components are the elongations λ_i . For fiber reinforced materials, an anisotropic approach must be used and a fiber direction vector \mathbf{M} is defined for each fiber orientation. This leads to the introduction of two new invariants, I_4 and I_5 which are defined as:

$$I_4 = \mathbf{MCM}, \quad I_5 = \mathbf{MC}^2\mathbf{M}. \quad (2)$$

Other invariants can be introduced if there are many reinforced directions.

Many hyperelastic materials, as arterial tissues, are often considered as incompressible. To overcome well-known numerical difficulties associated with the incompressibility condition, a nearly incompressible approach is usually adopted. This later approach leads to use the isovolume deformation gradient $\bar{\mathbf{F}} = J^{-1/3} \mathbf{F}$. Its principal components are thus defined by $\bar{\lambda}_i = J^{-1/3} \lambda_i$ ($i = 1, 2, 3$) and it permits to build incompressible invariants:

$$\bar{I}_1 = I_3^{-1/3} I_1, \quad \bar{I}_2 = I_3^{-2/3} I_2, \quad \bar{I}_4 = I_3^{-1/3} I_4, \quad \bar{I}_5 = I_3^{-2/3} I_5. \quad (3)$$

The strain energy density W is thus split into two parts, an isochoric one \bar{W} and a volumetric one U :

$$W = \bar{W}(\bar{I}_1, \bar{I}_2, \bar{I}_4, \bar{I}_5) + U(J). \quad (4)$$

The volume variation is then controlled by the choice of the volumetric function $U(J)$ which depends on the initial bulk modulus κ of the material.¹⁰ The incompressibility of the material is nearly reached when the volumetric energy U is greater than the isochoric energy \bar{W} , i.e., for large values of the bulk modulus κ which in this particular case serves as a user-specified penalty parameter. This last point is discussed in the following.

2.1.2. Strain energy densities for artery material

Within this framework, two forms of isochoric strain energy (\bar{W}) using exponential⁸ or polynomial⁹ functions were proposed in order to describe the experimentally observed hyperelastic anisotropic behavior of arteries.⁷ In these models, the material

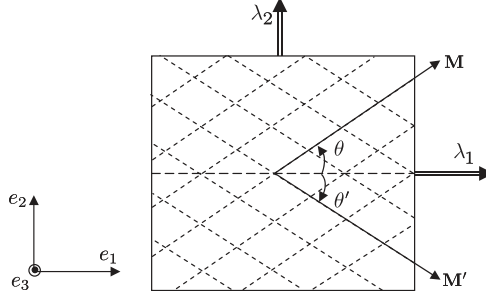


Fig. 1. Fibers orientation in the arterial wall.

is considered as a matrix material reinforced with two fiber networks (Fig. 1). Thus, two vectors are introduced to describe the two distinguished fiber orientations: $\mathbf{M} = (\cos \theta \ \sin \theta \ 0)$ and $\mathbf{M}' = (\cos \theta' \ \sin \theta' \ 0)$, with $\theta = -\theta'$. As a consequence, the strain energy density (W) may depend on the following anisotropic strain invariants defined for the two orientations, as:

$$\begin{aligned} \bar{I}_4 &= I_3^{-1/3} \mathbf{M} \mathbf{C} \mathbf{M}, & \bar{I}_5 &= I_3^{-2/3} \mathbf{M} \mathbf{C}^2 \mathbf{M}, & \bar{I}_6 &= I_3^{-1/3} \mathbf{M}' \mathbf{C} \mathbf{M}', \\ \bar{I}_7 &= I_3^{-2/3} \mathbf{M}' \mathbf{C}^2 \mathbf{M}', & \bar{I}_8 &= I_3^{-1/3} (\mathbf{M} \mathbf{M}') \mathbf{M} \mathbf{C} \mathbf{M}', & I_9 &= (\mathbf{M} \mathbf{M}')^2. \end{aligned} \quad (5)$$

In practice, \bar{I}_1 , \bar{I}_4 and \bar{I}_6 are usually sufficient to capture the typical features of arterial response.^{8,9,11}

In this study, models in consideration are:

- polynomial reinforcement constitutive equation (P6 model)

$$W = U(J) + c_1(\bar{I}_1 - 3) + \alpha(\bar{I}_1 - 3)^2 + k_1(\bar{I}_4 - 1)^6 + k_3(\bar{I}_6 - 1)^6, \quad (6)$$

where c_1 , α , k_1 and k_3 are material parameters. Basciano and Kleinstreuer⁹ recently proposed a similar form without the isotropic neo-hookean part. In this particular case, let us remark that there is no initial slope in the stress-strain curve ($c_1 = 0$), which can lead to numerical difficulties (nonconvergence).

- Rodriguez constitutive equation (R model)⁸

$$\begin{aligned} W &= U(J) + c_1(\bar{I}_1 - 3) \\ &+ \frac{k_1}{2k_2} \{ \exp[k_2[(1 - \rho)(\bar{I}_1 - 3)^2 + \rho(\bar{I}_4 - \bar{I}_4^0)^2]] - 1 \} \\ &+ \frac{k_3}{2k_4} \{ \exp[k_4[(1 - \rho)(\bar{I}_1 - 3)^2 + \rho(\bar{I}_6 - \bar{I}_6^0)^2]] - 1 \}, \end{aligned} \quad (7)$$

where k_2 and k_4 are dimensionless material parameters, ρ is a measure of anisotropy. \bar{I}_4^0 and \bar{I}_6^0 correspond to the initial crimping of the fibers. In the first model, the anisotropic term is assumed to contribute when either $\bar{I}_4 > 1$ or $\bar{I}_6 > 1$, or both.

Similarly, the term $(\bar{I}_i - \bar{I}_i^0)$ ($i = 4, 6$), does not contribute to the strain energy whether $\bar{I}_4 \leq \bar{I}_4^0$ or $\bar{I}_6 \leq \bar{I}_6^0$. This last model is equivalent to the model proposed by Holzapfel *et al.*¹¹ for $\rho = 1$ and $\bar{I}_i^0 = 1$.

A general form for the volumetric function (Eq. (8)) was proposed in Ref. 10.

$$U/\kappa = ((\alpha + 1)^{-1}J^{(\alpha+1)} + (\beta - 1)^{-1}J^{(1-\beta)})(\alpha + \beta)^{-1} - (\alpha + 1)^{-1}(\beta - 1)^{-1}, \quad (8)$$

where α and β are dimensionless parameters that can be used to obtain the most common volumetric functions proposed in the literature, $\alpha > 0$ and $\beta > 1$. In this work, the classical quadratic function¹² usually implemented in finite element analysis codes is chosen for the two material models:

$$U(J) = \frac{\kappa}{2}(J - 1)^2. \quad (9)$$

It was obtained with $\alpha = 1$ and $\beta = 0$ in Eq. (8). This volumetric function violates the condition on β , but as the deformation range investigated in this study leads to very small volume changes ($J \approx 1$), all the volumetric functions proposed in Ref. 10 coincide as we can observe in Fig. 2(a). Moreover, the evolution of the derivative of this ratio with the volume change is also illustrated in Fig. 2(b), since this derivative is involved in the stress calculation. Table 1 shows the values of α and β for the different volumetric functions in Fig. 2.

In order to control the material volume variation, one can choose an arbitrary higher initial bulk modulus. However, since this modulus must be considered as a material property, linking it to the material parameters seems to be coherent. For that purpose, we choose to come back to linear elasticity thanks to the well-known relationship between the initial bulk modulus κ , the Young's modulus and the Poisson's ratio. In the case of orthotropic materials, like the arterial wall, the initial bulk modulus can be expressed in term of the Poisson's ratio ν_{ij} , and Young's moduli E_i , E_j and E_k as follow¹³:

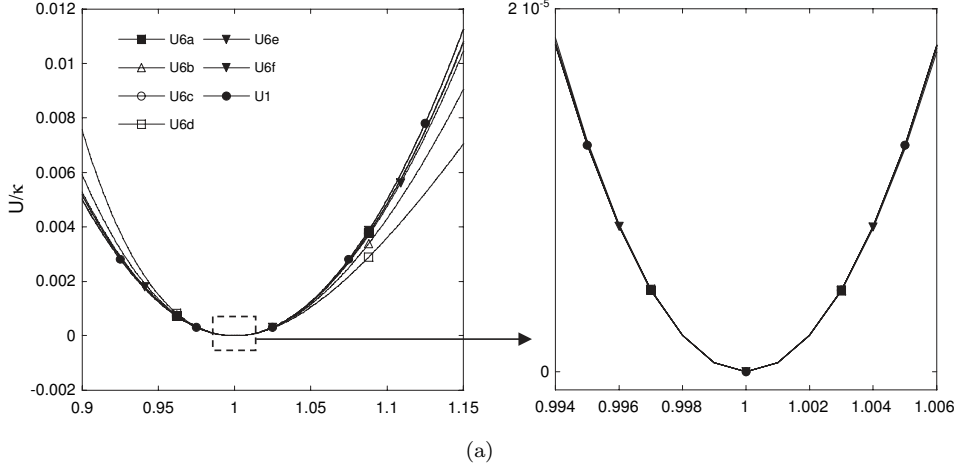
$$\kappa = \frac{E_i E_j E_k}{3[(1 - 2\nu_{ij})E_i E_k + E_j E_k - E_i E_j]}, \quad (10)$$

where $i \neq j \neq k$ ($i, j = 1, 2, 3$). For the sake of simplicity, the classical isotropic relationship often available in finite element codes is adopted in the following:

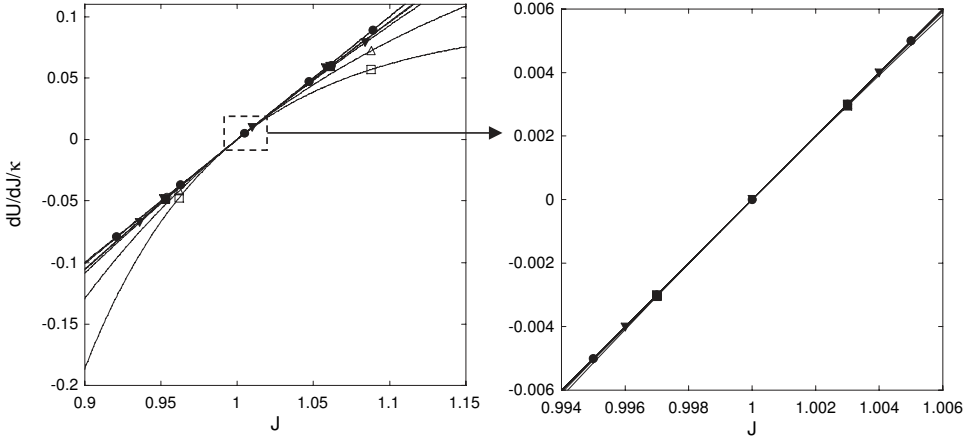
$$\kappa = \frac{E}{3(1 - 2\nu)}, \quad (11)$$

Table 1. Parameters for the volumetric function (Eq. (8)).¹⁰

U	U_1	U_{6a}	U_{6b}	U_{6c}	U_{6d}	U_{6e}	U_{6f}
α	1	2	0.001	1	0.001	2.3	0.45
β	0	2	3.790	1.001	10	1.4	1.05



(a)



(b)

Fig. 2. (a) Evolution of the ratio of the volumetric function to the initial bulk modulus with the volume change; (b) evolution of the derivative of the ratio of the volumetric function to the initial bulk modulus with the volume change.¹⁰

where E and ν are the Young's modulus and the Poisson's ratio. Due to this simplification, by convention we choose the \mathbf{e}_1 direction (Fig. 1) as reference for determining the Young's modulus in infinitesimal deformation of anisotropic materials under consideration. This choice has no consequence on the following analysis. The Poisson's ratio in (Eq. (11)) is a driving representative parameter of the compressibility (which has no physical relevance) and the strict incompressibility is reached

for $\nu = 0.5$. After some algebraic manipulations, it comes that:

- P6 model

$$E = 6c_1. \quad (12)$$

- R model

$$E = \frac{2}{1 + 2\frac{\rho k_1}{c_1} \sin^4 \theta} [3c_1 + 4\rho k_1 (\cos^4 \theta + \sin^4 \theta) - 4\rho k_1 \cos^2 \theta \sin^2 \theta]. \quad (13)$$

The material parameters for each model are given in Table 2. The material parameters for the exponential model were identified in Ref. 8 on biaxial tensile tests data from Ref. 7. Using these parameters, a Young's modulus of 264 kPa was obtained with (Eq. (13)). Let us remark that the fibers orientation, θ , in these models was considered as a phenomenological parameter, so its values have no physical relevance.⁸ For P6 model, to have the same Young's modulus as for R model, $c_1 = 44.0$ kPa was adopted. Thus, for a given value of the Poisson's ratio, we have the same initial bulk modulus for the two material models (Eq. (11)). The parametric study in the following is achieved with the initial bulk modulus, κ .

2.2. Equibiaxial loading

To study the different constitutive equations, a loading state close to that happens in arterial walls, i.e., equibiaxial loading, is chosen. The same elongation is imposed in the two plane directions ($\lambda_1 = \lambda_2$). The stress states are determined by means of the derivative of the strain energy density: $W_i = \partial W / \partial \bar{I}_i$ and $U_J = \partial U / \partial J$. The Cauchy stress formulation can be written as:

$$\begin{cases} \sigma_1 = \frac{2}{J} [(\bar{\lambda}_1^2 - \bar{\lambda}_3^2)W_1 + (W_4 + W_6)(\bar{\lambda}_1 \cos \theta)^2] \\ \sigma_2 = \frac{2}{J} [(\bar{\lambda}_2^2 - \bar{\lambda}_3^2)W_1 + (W_4 + W_6)(\bar{\lambda}_2 \sin \theta)^2] \\ \sigma_3 = \frac{2}{3J} [(3\bar{\lambda}_3^2 - \bar{I}_1)W_1 + \bar{I}_4(W_4 + W_6)] + U_J. \end{cases} \quad (14)$$

The third equation is used to determine the third elongation λ_3 by imposing a stress free condition $\sigma_3 = 0$, the plane stress assumption. For each model, the inversion of

Table 2. Material constants: P6 and R refer to P6 model and R model.

	c_1 (kPa)	α (kPa)	$k_1 = k_3$ (kPa)	$k_2 = k_4$	ρ	$\bar{I}_4^0 = \bar{I}_6^0$	θ ($^\circ$)	E (kPa)
P6	44.0	73.996	65500	—	—	—	44.60	264
R	0.12	—	244.90	1576.20	0.14	1.038	5.00	264

this later equation was numerically done using Matlab [®] for several values of the initial bulk modulus.

The evolution of the third elongation λ_3 versus the first one λ_1 for the different constitutive equations is presented in Figs. 3(a) and 3(b). These figures show that even if the initial bulk modulus is very large $\kappa \geq 1 \times 10^{17}$ kPa, the elongation may be very far from the incompressible case, namely for the R model. Moreover for this model, it appears that whatever the value of the initial bulk modulus the material is thickening after a given value of the deformation (beyond 10%), which is not physically acceptable. This is due to the fact that the volumetric function U is not increasing enough compared to the isochoric energy \bar{W} to satisfy the incompressibility condition. For the polynomial model, when $\kappa \geq 4.40 \times 10^6$ kPa, the material response is identical to the incompressible case, in the range of the considered deformation. These results are reinforced by the evolution of J versus λ_1 , presented in Figs. 3(c) and 3(d). It clearly appears that the volume variation can become very high, even if κ is very large. Nevertheless, the curves also highlight that the incompressibility hypothesis seems to be verified until a given level of deformation depending on the constitutive equation.

The near-incompressibility formulation has also a large consequence on the stress state as illustrated in Figs. 3(e) and 3(f), which show the evolution of the first principal stress σ_1 versus λ_1 for the different models. For a given value of λ_1 , an important difference can be observed between the incompressible theoretical stress, $\sigma_1(\text{inc})$, and the stress calculated for different values of the initial bulk modulus, $\sigma_1(\kappa)$. In order to better quantify this difference, the relative error defined as:

$$\text{Er} = \frac{\sigma_1(\text{inc}) - \sigma_1(\kappa)}{\sigma_1(\text{inc})} \quad (15)$$

for $\kappa = \{4.40 \times 10^4, 4.40 \times 10^6\}$ kPa, is plotted in Fig. 4 for the two constitutive models. All these results point out that to keep a constant volume during strain hardening, a high volumetric function is needed compared to the isochoric one. Obviously, this condition depends on both the expression of the volumetric energy and the value of the initial bulk modulus κ . In the present case, a classical quadratic expression for U (Eq. (9)) is used. However, the volumetric functions comparison in Fig. 2 shows that another volumetric function, in the range of deformation investigated, would lead to the same conclusion. Obtained results show that a large value of κ appears to be sufficient to satisfy the incompressibility condition for the P6 model in this range of deformation. When models become strongly nonlinear, as R model, large values of κ are sufficient to ensure the incompressibility condition in a restricted range of deformation. Consequently, numerical simulations outside this range of deformation can lead to large errors on the estimations of stresses in arterial wall. This point is illustrated in the next section in the particular case of AAA.

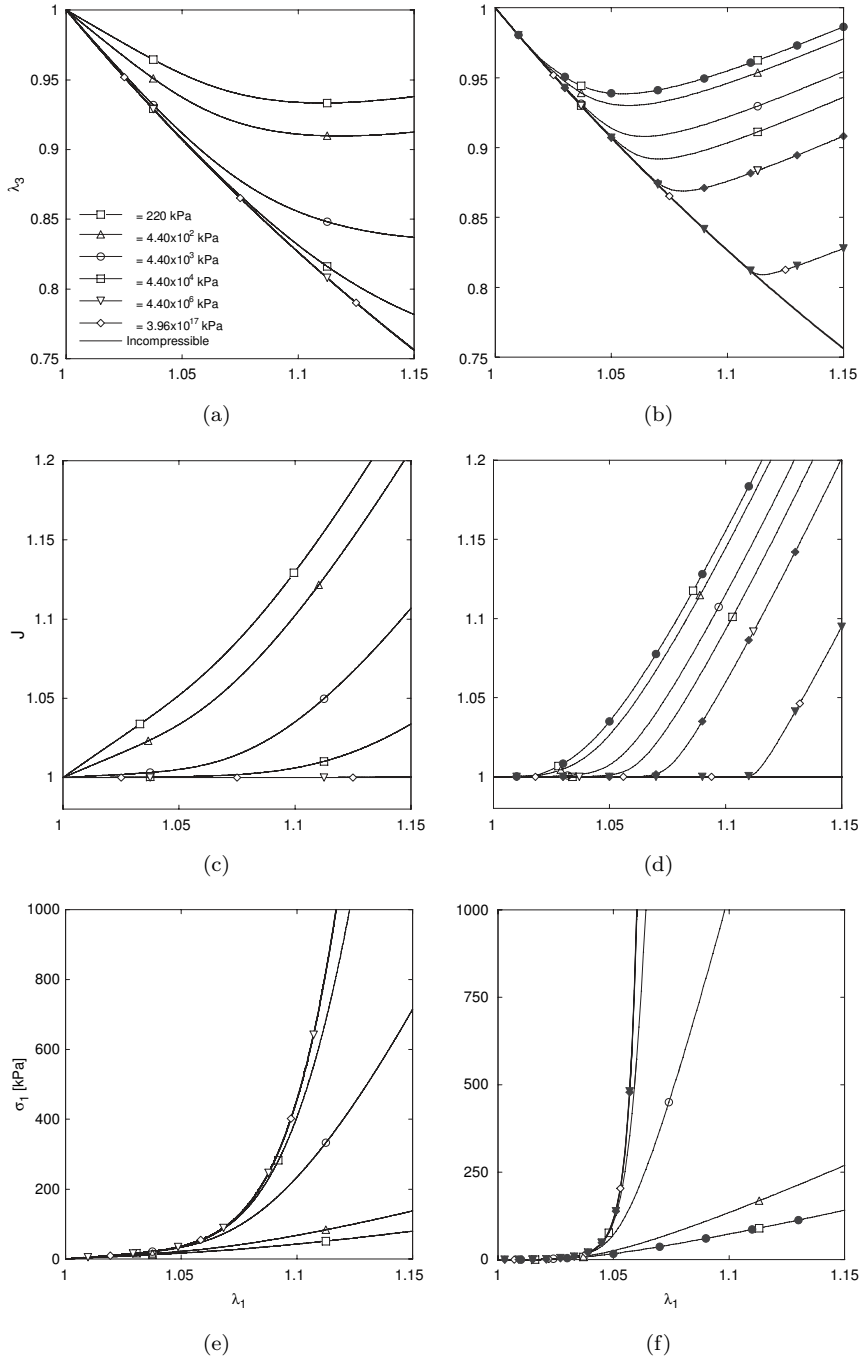


Fig. 3. Evolution of λ_3 , J and σ_1 versus $\lambda_1 (= \lambda_2)$ during an equibiaxial tensile test for different values of the initial bulk modulus: (a,c,e) P6 model, (b,d,f) R model, in this last case the gray filled marks correspond to results from the finite elements analysis.

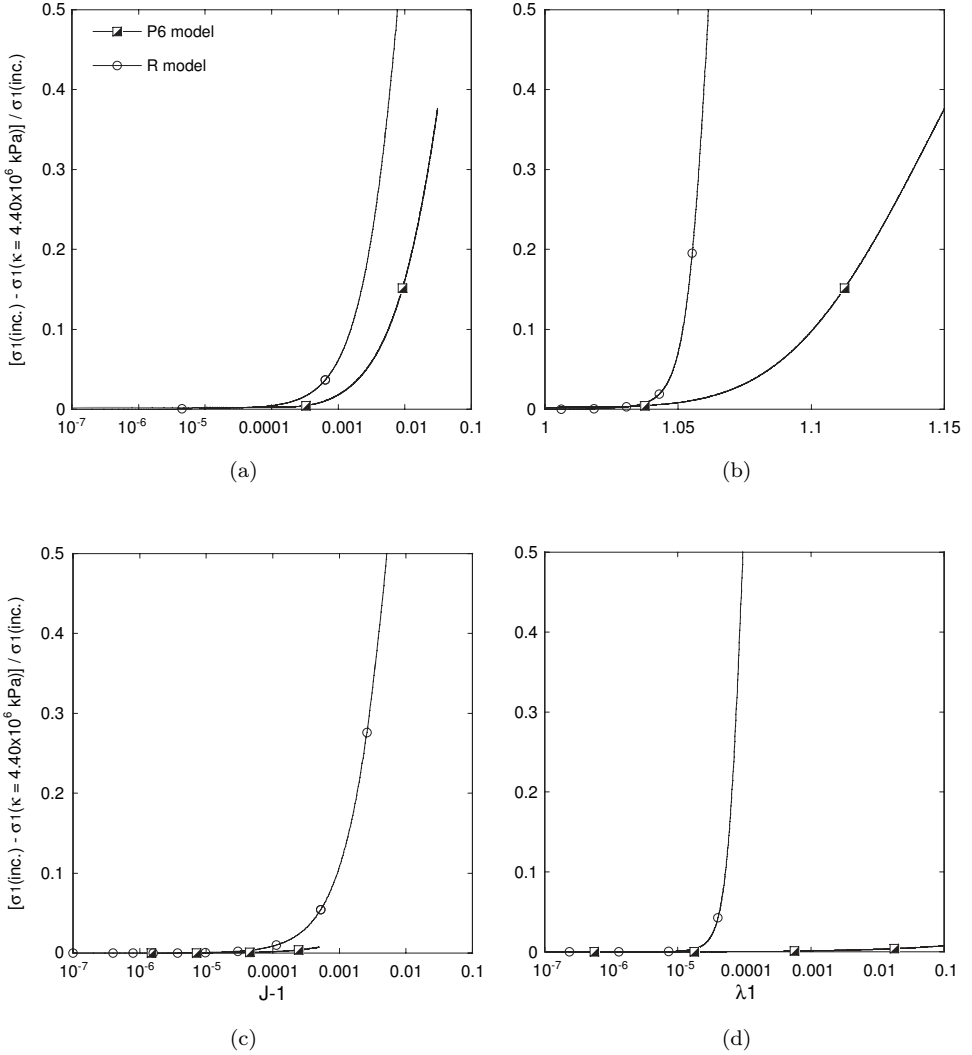


Fig. 4. Relative error (15) for (a) and (b): $\kappa = 4.40 \times 10^4$ kPa, (c) and (d) $\kappa = 4.40 \times 10^6$ kPa versus the volume change $J - 1$ (a,c) and the elongation λ_1 (b,d).

3. Compressibility Effects on Abdominal Aortic Aneurysm Wall Stress Analysis

The aim of this section is to investigate the influence of the near-incompressibility, i.e., the influence of the initial bulk modulus κ , on AAA wall stress distribution. For that purpose, the model recently proposed in Ref. 8 (Eq. (7)) was implemented in a finite element code and numerical simulations on idealized AAA models were performed.

3.1. Implementation and validation of the model

The model (Eq. (7)) was implemented in the finite element code Comsol Multiphysics $\text{\textcircled{R}}$. The near-incompressibility is formulated by using a mixed formulation — *pressure-displacement*-, with quadratic displacement and linear pressure Lagrangian’s elements. A direct solver (UMFPACK) was used for all the following simulations. As in Sec. 2, the classical volumetric energy U defined by the relation (Eq. (9)) is used and the initial bulk modulus is still given by (Eq. (11)).

In order to validate this implementation, equibiaxial tensile tests were first simulated for several values of the initial bulk modulus, from 220 to 3.96×10^{17} kPa. Figures 3(b), 3(d) and 3(f) show the evolution of λ_3 , J and σ_1 versus λ_1 . Let us remark that the directions $(\mathbf{e}_1, \mathbf{e}_2, \mathbf{e}_3)$ in the biaxial test correspond to $(\mathbf{e}_\theta, \mathbf{e}_z, \mathbf{e}_r)$ in the arterial wall. We can observe a perfect agreement between analytical solutions (continuous line) and finite element results (gray filled marks) in the whole range of deformation.

3.2. Finite element analysis of AAA wall stress

3.2.1. Geometry

Finite element analysis was performed on idealized AAA models (Fig. 5) whose mathematical form was proposed in Ref. 8. Briefly, the model is characterized by the aneurysm dilatation parameter ($F_r = R_{\text{an}}/R_a$), its eccentricity ($F_e = e/((F_r - 1)R_a)$) and its aspect ratio ($F_\ell = L_{\text{an}}/R_{\text{an}}$), where R_a is the healthy aorta radius, R_{an} the aneurysm maximal radius, e the deviation of the aneurysm axis from the the healthy aorta axis and L_{an} defines the aneurysm length. In the following, the aneurysm aspect ratio ($F_r = 2.5$), its total length ($L = 100$ mm), the wall thickness ($t = 1.5$ mm), the healthy aorta radius ($R_a = 10$ mm) and the dilatation parameter ($F_r = 2.75$) are assumed to be constant. This value of the dilatation parameter corresponds to a maximum diameter of 5.5 cm of the aneurysm. The CAO models were built in SolidWorks $\text{\textcircled{R}}$ and then imported into the finite element analysis software. In the above model, the middle section in the plane (x, y) constitutes a plane of symmetry. Therefore, only the upper part of the model was used in the finite element analysis. The full model can be reconstructed after.

3.2.2. Mesh

As mentioned above, a *pressure-displacement* (U-P) formulation, inherent to the near-incompressibility assumption, was adopted. Consequently, P2-P1 elements (i.e., quadratic and linear interpolation for the displacement and the pressure, respectively) are used. These elements are fully integrated which results in zero hourglass energy.

Mesh-influence studies indicated that the numerical results are less dependent on the number of elements along the aneurysm axis. On the other side, the number

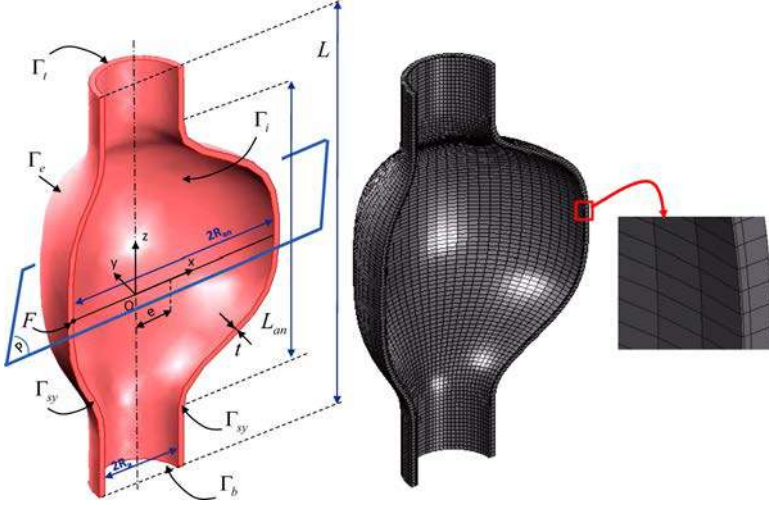


Fig. 5. AAA geometrical model and boundaries designation and mesh model.

Table 3. Influence of the mesh discretization (regular mesh) within the AAA thickness (axisymmetric model).

Number of elements	2	3	4	6	8	10
$\sigma_{1\max}$ (kPa)	565	624	652	676	685	690

of elements in the AAA wall thickness can strongly affect the numerical results. In order to capture the strong stress gradient within the AAA thickness (close to the inner surface of the aneurysm in the case of the anisotropic model (7)), several simulations were performed by increasing the number of elements from 2 to 10 (the thickness of each element being the same). The obtained numerical results (Table 3) show that the influence of the mesh becomes negligible (less than 2 %) when the number of elements is larger than 6. In order to reduce the computational time, we found that similar results can be obtained by using only three elements but not with the same size. Precisely a structured mesh was adopted (Fig. 5) with three elements across the AAA wall thickness, 36 elements in the orthoradial direction and 60 elements along the AAA axis. The thickness of the element close to the inner surface of the aneurysm is much thinner (10 times) than the one close to the outer surface (Fig. 5). Using this type of mesh, we found that $\sigma_{1\max} = 698$ kPa.

3.2.3. Collagen fibers orientation in nonsymmetric AAA models

The model implementation was validated in § 3.1 for equibiaxial tensile tests. The difficulty in the case of an aneurysm, namely a nonsymmetric AAA geometrical

model, is the definition of the fibers orientation in the arterial wall. For that purpose, on the aneurysm internal surface, the two tangential vectors (\mathbf{T}_1 and \mathbf{T}_2) were extruded through the arterial wall thickness to make them available at every integration point. These two vectors were then used to define a local orientation of the collagen fiber. This process is accomplished by using the “Extrusion Coupling Variables” in Comsol Multiphysics $\text{\textcircled{R}}$.

3.2.4. Boundary conditions

The following boundary conditions are applied on the AAA model (Fig. 5):

$$\left\{ \begin{array}{ll} u_z = 0 & \text{on } \Gamma_t \text{ and on } \Gamma_{sz} \\ u_y = 0 & \text{on } \Gamma_{sy} \\ u_x = 0 & \text{at the corner } F \\ \boldsymbol{\sigma} \cdot \mathbf{n} = P\mathbf{n} & \text{on } \Gamma_i \\ \boldsymbol{\sigma} \cdot \mathbf{n} = \mathbf{0} & \text{on } \Gamma_e \end{array} \right. \quad (16)$$

In the proximal face Γ_t ($z = L/2$), a free radial displacement and a zero-axial displacement ($u_z = 0$) were imposed, instead of embedding boundary conditions which lead to stresses concentration in this region of the AAA as in Refs. 8 and 14. A symmetry condition is applied on both the planes Γ_{sz} ($z = 0$) and Γ_{sy} ($y = 0$). The usual systolic pressure ($P = 120\text{mmHg}$) was applied in the inner surface (Γ_i) of the aneurysm and the outer side (Γ_e) is stress free.

3.2.5. Wall stress in an axisymmetric AAA

In this section, the first principal stress is evaluated in idealized AAA geometries by using hyperelastic anisotropic model for the arterial wall. The way the near-incompressibility assumption affects this stress distribution and its maximum value in the aneurysm is emphasized. For that purpose, the stress evolution and the material volume variation are studied when the initial bulk modulus (κ), which controls the material compressibility, varies from its classical values to very large values.

Figure 6 shows the distribution of the first principal stress σ_1 (which is closely aligned to $\sigma_{\theta\theta}$) and the jacobian J in the AAA for three different values of κ . Correspondence between the values of κ and those of ν is given in Table 4. For the clarity, one-half of the aneurysm reconstructed from 2D-axisymmetric simulations is shown on these figures. We can observe that:

- both the distribution and the magnitude of the first principal stress σ_1 are strongly affected by the value of κ . When $\kappa = 4.40 \times 10^3$ kPa, Fig. 6 illustrates that the maximum first principal stress $\sigma_{1\max}$ is located in the inner surface at the junction between the aorta and the aneurysm and does not exceed 393 kPa. By increasing the value of the initial bulk modulus, the location of $\sigma_{1\max}$ moves

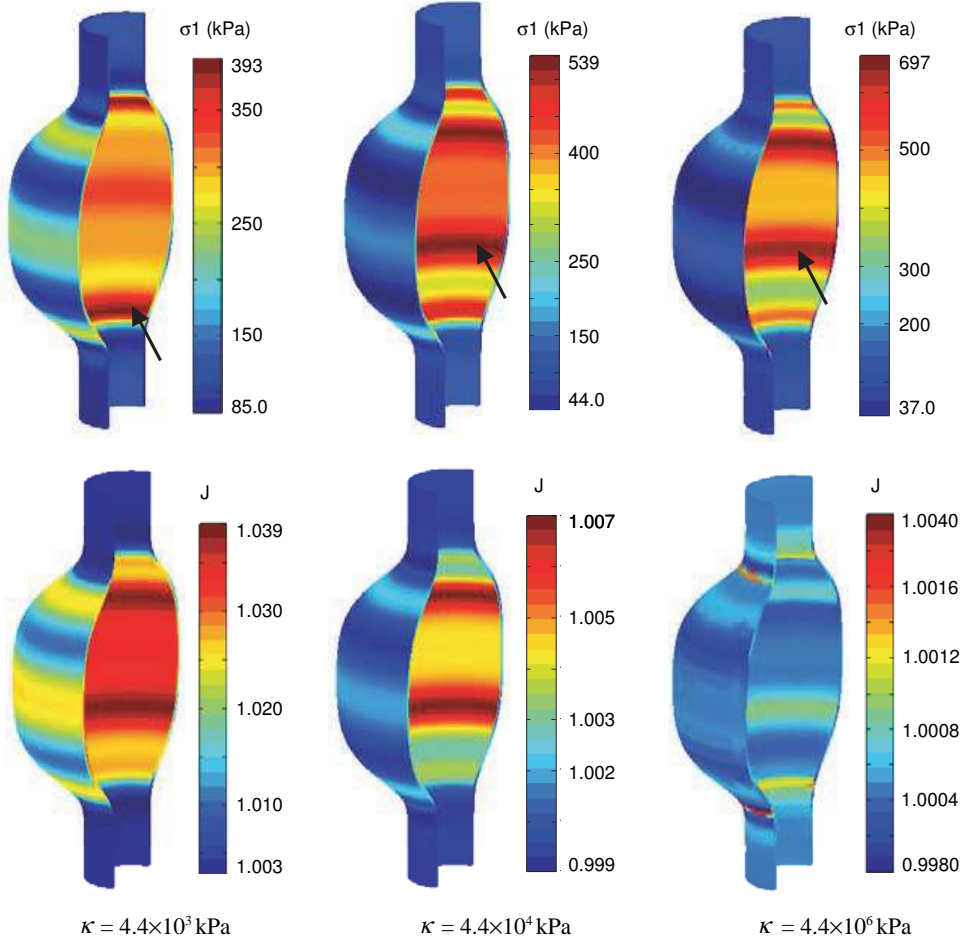


Fig. 6. 3D representation of an axisymmetric simulations results: Distribution of σ_1 and J in the AAA. The arrow indicates the location of $\sigma_{1\max}$.

Table 4. $\sigma_{1\max}$ in the AAA versus κ (or ν).

κ (kPa)	ν	J_{\max} (%)	$\sigma_{1\max}$ (kPa)	Er(%)
4.40×10^3	0.49000	3.90	393	44
4.40×10^4	0.49900	0.70	539	24
4.40×10^5	0.49990	0.40	675	4.0
4.40×10^6	0.49999	0.40	698	0.4
3.96×10^{17}	$0.5 - 1 \times 10^{-16}$	0.40	701	—

towards the center of the bulged part of the AAA and its magnitude is almost multiplied by two for $\kappa = 4.40 \times 10^6 \text{ kPa}$.

- The distribution of the volume variation parameter J (Fig. 6) is also dependent on the initial bulk modulus. As expected, its magnitude decreases with

increasing κ and tends towards the incompressibility case ($J = 1$) in the whole AAA for the largest value of κ . The maximum volume variations which are located in the bulged part of the AAA are typically the order of 3.9% and 0.04% for $\kappa = 4.40 \times 10^3$ kPa and $\kappa = 4.40 \times 10^6$ kPa, respectively.

These results point out that significant errors can be made on the peak wall stress estimation (magnitude and location) even in a simple AAA geometry when the incompressibility condition is not fulfilled. Such effects could be amplified in the case of patient-specific AAA models which present more complex geometric features. The numerical values deduced from this analysis are summarized in Table 4. Beside the very small volume variation (less than 1% beyond $\kappa = 4.40 \times 10^4$ kPa), the maximum first principal stress could deviate with about 24% from the incompressibility case. This is due to the strong nonlinearity of the mechanical model (Eq. (7)). As Fig. 7 clearly shows, the magnitude of $\sigma_{1\max}$ in the AAA wall rapidly increases with increasing κ and tends towards a plateau, when κ is larger than $\kappa = 4.40 \times 10^6$ kPa. This value ensures an estimation of $\sigma_{1\max}$ with an error lower than 1%, whereas a value of $\kappa = 4.40 \times 10^5$ kPa may lead to errors close 4%. Finally, let us remark that the maximal first principal stress obtained in Ref. 8 for the same AAA model with a normal systolic pressure is about $\sigma_{1\max} = 520$ kPa. This value is 26% smaller than the value at the plateau (Fig. 7). The value of $\kappa = 3.96 \times 10^{17}$ kPa was assumed to be the incompressible case since it corresponds to the limit of the numerical precision of the finite element analysis software used. Anyway, for the anisotropic model under consideration, we can observe that beyond $\kappa = 4.40 \times 10^6$ kPa, $\sigma_{1\max}$ reaches a stable value.

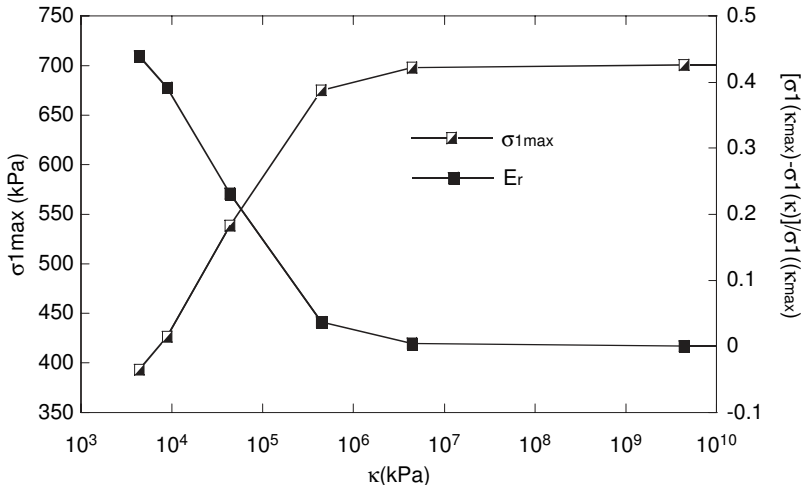


Fig. 7. Evolutions of $\sigma_{1\max}$ and errors on its values E_r (Eq. (15)) in terms of the initial bulk modulus κ .

3.2.6. Effects of non-symmetrical AAA geometry on the wall stress

The above results were obtained for an axisymmetric AAA model while due to the surrounded organs, especially the spine, the abdominal aortic aneurysm does not usually preserves its initial fusiform geometry. The loss of symmetry in the aneurysm is measured by the eccentricity parameter (F_e) which varies from 0 (axisymmetric model) to 1 (“fully” nonsymmetric model). Figure 8 exhibits σ_1 distribution for $F_e = \{0.0, 0.5, 1.0\}$. Unlike the symmetric model, $\sigma_{1\max}$ is located in the posterolateral surface, close to the junction of the bulged part and the healthy aorta. The risk of the aneurysm rupture is very high in these two locations as reported in Refs. 4 and 15. Here, only results for $\kappa = 4.40 \times 10^6$ kPa are presented since $\sigma_{1\max}$ location does not change beyond the classical value of the initial bulk modulus (4.40×10^4 kPa, Fig. 6). However, the magnitude of the first principal stress is strongly modified with both the aneurysm eccentricity and the initial bulk modulus. Figure 8 shows the modification of σ_1 pattern and the increase of $\sigma_{1\max}$ with the aneurysm eccentricity. This increase is nearly linear for $F_e \leq 0.75$ and nonlinear after (Fig. 9). In our best knowledge, such nonlinearity in $\sigma_{1\max}$ increase with the aneurysm eccentricity was not observed before, precisely when using hyperelastic anisotropic material model. We also reported values of $\sigma_{1\max}$ obtained by Rodriguez *et al.*⁸ in Fig. 9. With the same geometrical and mechanical models, these authors found a linear increase of $\sigma_{1\max}$ with the aneurysm eccentricity increase. According to their results, $\sigma_{1\max}$ increases with 33% from an axisymmetric aneurysm to a fully nonsymmetric one. By contrast, our results exhibit an increase of $\sigma_{1\max}$ of about 135% when $\kappa = 4.40 \times 10^6$ kPa. Thus, for this value of κ and for the fully non-symmetric AAA model, in comparison to Ref. 8 the error committed (Eq. (15)) on the maximum stress is about 58%. When the same analysis is performed with $\kappa = 4.40 \times 10^4$ kPa, we found an increase of 109% for $\sigma_{1\max}$. In this case, for $F_e \leq 0.5$, our results

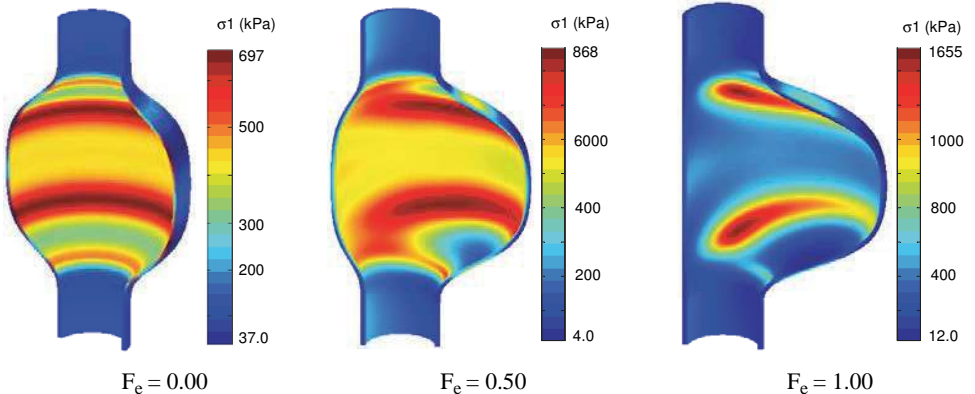


Fig. 8. Distribution of the first principal stress σ_1 in nonsymmetric AAA geometry when the initial bulk modulus $\kappa = 4.40 \times 10^6$ kPa.

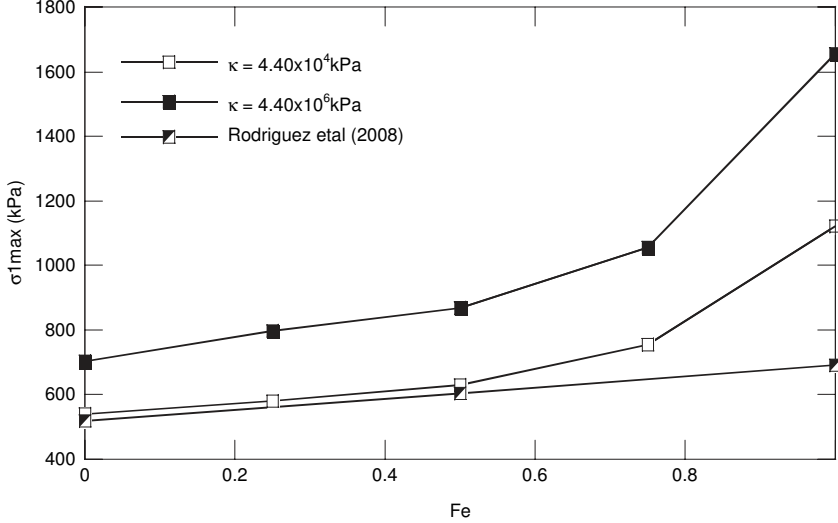


Fig. 9. $\sigma_{1\max}$ evolution versus the aneurysm eccentricity, results from Ref. 8 were reported.

are the same order of magnitude of those in Ref. 8, see Fig. 9. Therefore, it seems that their results would correspond to an initial bulk modulus of about 4.40×10^4 kPa. However, even with this value of κ , the discrepancy between the two values of $\sigma_{1\max}$, for $F_e = 1.0$, is about 38%. This could be explained by the fact that in Ref. 8, $\sigma_{1\max}$ was only considered in the bulged region of the aneurysm.

The material model (Eq. (7)) used in our finite element analysis was identified in Ref. 8 thanks to experimental data on AAA tissues from Ref. 7. However, whatever the geometrical model studied here, the obtained maximum stresses are very large compared to those reported from Ref. 7, about 120 kPa. This remark remains valid for many previous works.^{7,8,16} Nevertheless, our results are the same order of magnitude as those obtained by Rissland *et al.*¹⁷ in patient-specific AAA models (with an anisotropic material model and with a uniform AAA wall thickness of 2 mm). Namely in the fully nonsymmetric idealized AAA model ($F_e = 1.0$), we found $\sigma_{1\max} = 1654$ kPa while these authors reported a maximum Von Mises stress of 1555 kPa. Finally, let us remark that these peak values of the first principal stress are about 30% higher than those measured by Raghavan *et al.*¹⁸ in orthoradial direction of AAA tissues ($\sigma_{\text{ultimate}} \approx 1200$ kPa, in uniaxial tensile tests).

4. Concluding Remarks

Accurate and reliable numerical stress analysis of AAA requires suitable constitutive models for the arterial material. For that purpose, hyperelastic anisotropic models were recently proposed to capture the main features of the experimentally

observed mechanical response of arterial tissues. In these models, arterial material are usually assumed to be incompressible and material parameters are identified in this way. In practice, a nearly incompressible approach, i.e., a mixed formulation *pressure-displacement*, to perform finite element simulations is usually adopted. Consequently, the strain energy is split into an isochoric part \bar{W} and a volumetric part U , which depends on J and on the initial bulk modulus κ of the material. This parameter is used to control the material volume variation.¹⁰

In this work, an analytical analysis of the influence of κ on the mechanical response of two invariant-based anisotropic models was first performed in the case of an equibiaxial tensile test. In each model, a quadratic volumetric function usually implemented in many finite element softwares was considered. Analytical results clearly show that, in that case, large values of κ are sufficient to ensure the incompressibility condition, i.e., to estimate wall stress with a reasonable precision, in a restricted range of deformations only. Such results were then confirmed through a finite element stress analysis of idealized AAA geometries by using the model proposed in Ref. 8. Numerical results in the axisymmetric AAA model show that too small values of κ may lead to important error on the magnitude of the maximum first principal stress and also on its location. In the present case, it is shown that a value of the initial bulk modulus larger than 4.40×10^6 kPa is sufficient to estimate wall stresses with an error smaller than 1%. This value of κ is 10 to 100 times larger than values used in some previous numerical analyzes.^{11,19}

In comparison to the maximum diameter criterion usually adopted for the aneurysm potential rupture, the maximum stress in the AAA wall is considered to be a more reliable indicator.²⁰ The above results illustrate that the aneurysm eccentricity could hugely contribute to this stress increase. However, the wall stress being mainly evaluated numerically, a particular care may be taken to include appropriate numerical, mechanical and geometrical parameters in order to obtain more realistic estimations. As we observed, from an axisymmetric to a fully non-symmetric AAA models, the maximum stress could increase with about 135% (from 702 kPa to 1655 kPa). When the near-incompressibility condition is not fulfilled, the relative error on $\sigma_{1\max}$ varies from 24% to 44%. To obtain convenient numerical predictions of the aneurysm wall stress, the above underlined errors must be fixed. Moreover, material models have to be identified on average patient data.

References

1. Humphrey JD, Taylor CA, Intracranial and abdominal aortic aneurysms: Similarities, differences, and need for a new class of computational models, *Annu Rev Biomed Eng* **10**:221–46, 2008.
2. Carew TE, Vaishnav RN, Patel DJ, Compressibility of the arterial wall, *Circ Res* **23**:61–68, 1968.
3. He CM, Roach MR, The composition and mechanical properties of abdominal aortic aneurysms, *J Vasc Surg* **20**:6–13, 1994.

4. Raghavan ML, Vorp DA, Toward a biomechanical tool to evaluate rupture potential of abdominal aortic aneurysm: Identification of a finite strain constitutive model and evaluation of its applicability, *J Biomech* **33**:475–482, 2000.
5. Thubrikar MJ, Labrosse M, Robicsek F, Al-Soudi J, Fowler B, Mechanical properties of abdominal aortic aneurysm wall, *J Med Eng Tech* **25**:133–142, 2001.
6. Xiong J, Wang SM, Zhou W, Guo Wu J, Measurement and analysis of ultimate mechanical properties, stress-strain curve fit, and elastic modulus formula of human abdominal aortic aneurysm and nonaneurysmal abdominal aorta, *J Vasc Surg* **48**:189–195, 2008.
7. Vande Geest JP, Sacks MS, Vorp DA, The effects of aneurysm on the biaxial mechanical behavior of human abdominal aorta, *J Biomech* **39**:1324–1334, 2006.
8. Rodriguez J, Ruiz C, Doblare M, Holzapfel GA, Mechanical stresses in abdominal aortic aneurysms: Influence of diameter, asymmetry, and material anisotropy, *J Biomech Eng* **130**:1–10, 2008.
9. Basciano CA, Kleinstreuer C, Invariant-based anisotropic constitutive models of the healthy and aneurysmal abdominal aortic wall, *J Biomech Eng* **131**:1–11, 2009.
10. Doll S, Schweizerhof K, On the development of volumetric strain energy functions, *J Appl Mech* **67**:17–21, 2000.
11. Holzapfel GA, Gasser TC, Ogden RW, A new constitutive framework for arterial wall mechanics and a comparative study of material models, *J Elasticity* **61**:1–48, 2000.
12. Simo JC, A framework for finite strain elastoplasticity based on maximum plastic dissipation and the multiplicative decomposition: Part I. Continuum formulation, *Comput Methods Appl Mech Eng* **66**:199–219, 1988.
13. Itskov M, Aksel N, Elastic constants and their admissible values for incompressible and slightly compressible anisotropic materials, *Acta Mech* **157**:81–96, 2002.
14. Scotti CM, Jimenez J, Muluk SC, Finol EA, Wall stress and flow dynamics in abdominal aortic aneurysms: Finite element analysis vs. fluid-structure interaction, *Comput Met Biomech Biomed Eng* **11**:301–22, 2008.
15. Xenos M, Rambhia SH, Alemu Y, Einav S, Labropoulos N, Tassiopoulos A, Ricotta JJ, Bluestein D, Patient-based abdominal aortic aneurysm rupture risk prediction with fluid structure interaction modeling, *Ann Biomed Eng* **38**:3323–3337, 2010.
16. Vande Geest JP, Schmidt DE, Sacks MS, Vorp DA, The effects of anisotropy on the stress analyses of patient-specific abdominal aortic aneurysms, *Ann Biomed Eng* **36**:921–32, 2008.
17. Rissland P, Alemu Y, Einav S, Ricotta J, Bluestein D, Abdominal aortic aneurysm risk of rupture: Patient-specific fsi simulations using anisotropic model, *J Biomech Eng* **131**:1–10, 2009.
18. Raghavan ML, Webster MW, Vorp DA, *Ex vivo* biomechanical behavior of abdominal aortic aneurysm: Assessment using a new mathematical model, *Ann Biomed Eng* **24**:573–82, 1996.
19. Peyraut F, Renaud C, Labebe N, Feng ZQ, Modélisation des tissus biologiques en hyperélasticité anisotrope — étude théorique et approche éléments finis, *C R Méc* **337**:101–106, 2009.
20. Fillinger MF, Marra SP, Raghavan ML, Kennedy FE, Prediction of rupture risk in abdominal aortic aneurysm during observation: Wall stress versus diameter, *J Vasc Surg* **37**:724–732, 2003.